Journal of Electronic Materials (2023) 52:7068–7073
https://doi.org/10.1007/s11664-023-10665-7

TOPICAL COLLECTION: 2022 U.S. WORKSHOP ON PHYSICS AND CHEMISTRY OF II-VI MATERIALS

Demonstration of T2SLs InAs/InAsSb Based Interband Cascade Detector Supported by Immersion Lens for LWIR

Waldemar Gawron[1,2] · Łukasz Kubiszyn[2] · Krystian Michalczewski[2] · Jarosław Jureńczyk[2] · Józef Piotrowski[2] · Piotr Martyniuk[1]

Received: 14 December 2022 / Accepted: 1 August 2023 / Published online: 29 August 2023

Abstract
This paper presents the performance of an interband cascade long-wavelength infrared detector designed for high operating temperatures supported by immersion lenses. The device is based on the "Ga-free" InAs/InAsSb type-II superlattice with highly doped p^+/n^+ superlattice tunneling junctions connecting adjacent stages. Detectivity of the multi-junction heterostructure detector exceeding 10^{10} cm $Hz^{1/2}/W$ was estimated at wavelength $\lambda \sim 9$ µm and $T = 210$ K and $\sim 3 \times 10^8$ cm $Hz^{1/2}/W$ for $T = 300$ K, achieving a tenfold improvement in detectivity in comparison to a device without an immersion lens and 30-fold improvement in detectivity in comparison to the single-stage device.

Keywords Interband cascade detector · InAs/InAsSb superlattice · T2SLs · HOT

Introduction

To fabricate a detector achieving optimal performance, the device design rules should be very simple and straightforward. The absorber must be optimized for the best α/g_{th} ratio (where $\alpha$is the absorption coefficient and $g_{th}$is the thermal generation rate) at a given wavelength (λ) and operating temperature (T). In the case of long-wave infrared radiation (LWIR) photodiodes operating at higher operating temperature (HOT) conditions, the optimized absorber thickness (comparable to the absorption depth ~ $1/\alpha$) is usually thicker than the carrier diffusion length, meaning that only a limited portion of photogenerated carriers contribute to the quantum efficiency (QE), which significantly limits the potential performance. Taking that into consideration, the active layer thickness must be less than the ambipolar diffusion length of the carriers. That problem could be circumvented by using a multi-junction structure developed and demonstrated based on bulk materials by Piotrowski et al.,[1] where thin absorbers with thickness comparable to the carrier diffusion length were connected in series, making the total thickness of all absorbers close to the radiation absorption depth (~$1/\alpha$). An example of the multi-junction device is an interband cascade photodetector (ICP) built of active, relaxation and tunneling regions based on the InAs/GaSb and InAs/InAsSb type-II superlattices (T2SLs) originally presented by Yang et al.[1–5] Yang et al. demonstrated ICIP with an AlSb/GaSb tunneling region connecting adjacent stages with T2SLs InAs/GaSb active layers. In our approach, we simplified the connecting/tunneling region by using a highly doped p^+/n^+ tunnel junction based on the same material as the active layer (in terms of the bandgap energy)—T2SLs "Ga-free" InAs/InAsSb. The ICIP structure itself, if properly designed, should increase performance in terms of the quantum efficiency and shot noise suppression, leading to higher detectivity (D^*). Further performance improvement could be obtained by increasing the optical area (A_o) to electrical area (A_e) ratio by implementation of the immersion lens, where detectivity scales (n^2, where n is the GaAs refractive index) according to the equation:

$$D^*_{\text{Peak}} \sim \left(\frac{A_o}{A_e}\right)^{1/2}. \quad (1)$$

✉ Piotr Martyniuk
piotr.martyniuk@wat.edu.pl

[1] Institute of Applied Physics, Military University of Technology, 2 Kaliskiego St., 00-908 Warsaw, Poland

[2] VIGO Photonics S.A., 129/133 Poznańska St., 05-850 Ożarów Mazowiecki, Poland

In this paper, the GaAs hyperhemispherically immersed multi-junction device is demonstrated, with increased A_o/A_e ratio and improved D^*. The detector structure was grown by molecular beam epitaxy (MBE) on a 1.1 mm-thick GaAs substrate (converted into a hyperhemispherical immersion lens) based on a T2SLs InAs/InAsSb absorber, bulk barrier layer and highly doped n^+/p^+ T2SLs InAs/InAsSb connecting regions. Detectivity of the multi-junction heterostructure detector exceeding 10^{10} cm $Hz^{1/2}/W$ was measured at wavelength, $\lambda \sim 9$ µm and $T = 210$ K [three-stage thermoelectric (TE) cooling] and $\sim 3 \times 10^8$ cm $Hz^{1/2}/W$ for $T = 300$ K, achieving a tenfold improvement in detectivity in comparison to the device without the immersion lens and 30-fold improvement in D^* in comparison to the single-stage device with net active layer thickness of 2.2 µm, comparable to the net thickness of the three-stage cascade detector.

Detector Architecture

The series of T2SLs InAs/InAsSb-based detectors, including one-stage (2.2 µm-thick absorber) and three-stage (1.86 µm-thick net absorber) cascade multi-junction structures, were grown by a RIBER Compact 21-DZ solid source MBE system, on 2″ semi-insulating 1.1 mm-thick GaAs (001) substrates, and are presented in Fig. 1.[6,7] The 250 nm GaAs smoothing layer was deposited, and next a 1 µm-thick GaSb buffer layer was grown by the IMF technique. The structure was built of the single 0.62 µm-thick absorber (9.99 nm period "Ga-free" T2SLs: InAs 7.58 nm/InAsSb 2.41 nm, $x_{Sb} = 0.38$), 0.59 µm-thick N^+ contact layer, 0.21 µm interface/gradient layers, bulk barrier, highly doped 0.175 µm p^+/n^+ tunneling regions and 0.12 µm p^+ top contact layer.

Several multi-stage cascade structures have been proposed based on T2SLs InAs/GaSb and InAs/InAsSb active layers, relaxation and tunneling regions e.g. AlAs/GaSb making the detector difficult to grow. In this work, the adjacent stages were connected by a traditional highly doped p^+/n^+ tunneling junction built the same as the active layer T2SLs InAs/InAsSb (the same bandgap energy) supported by the grading layer to facilitate tunneling. The schematic energy band diagram of the LWIR InAs/InAsSb T2SL multi-junction cascade detector with the p^+/n^+ tunneling region connecting stages under unbiased and HOT conditions is presented in Fig. 2 (region colors correspond to the structures presented in Fig. 1). The Si and Be dopants: $N_D \sim 10^{19}$ cm^{-3} and $N_A \sim 2 \times 10^{19}$ cm^{-3} for n^+ (45 nm) and p^+ layers (130 nm) were used during the MBE growth, respectively.

Detector Performance

The current–voltage (J_{Dark}–V) characteristics and differential resistance (R) were measured for 3-TE (210 K) for the three-stage immersed detector and are presented in Fig. 3a. For bias $V = -100$ mV, J_{Dark} was ~ 375 mA with corresponding

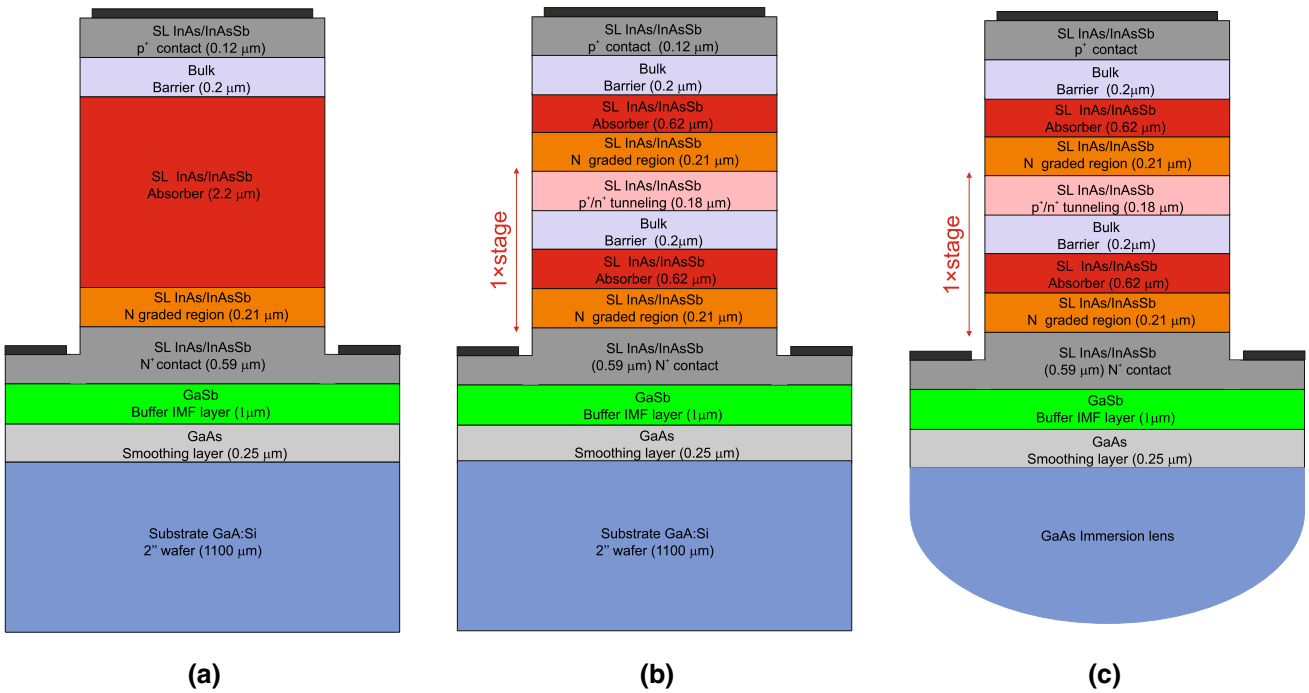

Fig. 1 The LWIR T2SL InAs/InAsSb barrier detector (single-stage detector) (**a**), multi-junction, three-stage cascade detector with p^+/n^+ connecting regions (**b**) and three-stage cascade detector with p^+/n^+ connecting regions supported by GaAs immersion lens (**c**).

$R \sim 540\ \Omega$. The $\lambda_{\text{cut-off}} \sim 10.5\ \mu\text{m}$ at 210 K was extracted from the spectral response curves and is presented in Fig. 3b. For $\lambda_{\text{Peak}} \sim 8\ \mu\text{m}$ the current responsivity reaches ~ 0.6 A/W while the detectivity reaches ~ 10^{10} cm $\text{Hz}^{1/2}$/W for the GaAs hyperhemispherically immersed detector and unbiased conditions, respectively.

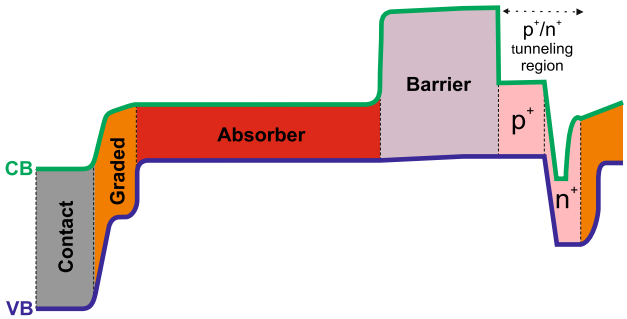

Fig. 2 The schematic energy band diagram of the LWIR InAs/InAsSb T2SL multi-junction cascade detector with p^+/n^+ tunneling region connecting stages for unbiased and HOT conditions.

The highly doped n^+/p^+ T2SLs InAs/InAsSb tunneling junction connecting adjacent stages generally slightly deteriorates the long-wavelength response. Since that region is thinner than the active layer, it does not influence D^*. This is a trade-off between long-wave spectral response and material growth complexity. One order of magnitude improvement in D^* scaling with ~ n^2 (n—GaAs refractive index) was reached in comparison to the detector without the immersion lens as presented in Fig. 3b.

For comparison purposes, Fig. 4 presents results for 230 K reached by 2-TE. For bias $V = -100$ mV, J_{Dark} was 1.7 mA with corresponding $R \sim 88\ \Omega$. For $\lambda_{\text{Peak}} \sim 7.3\ \mu\text{m}$, the current responsivity reaches 0.25 A/W with detectivity of 3.6×10^9 cm $\text{Hz}^{1/2}$/W for unbiased conditions, respectively. Room temperature performance is presented in Fig. 5, where for bias $V = -100$ mV, J_{Dark} was 5.1 mA with corresponding $R \sim 23\ \Omega$. For $\lambda_{\text{Peak}} \sim 7.5\ \mu\text{m}$, the current responsivity reaches

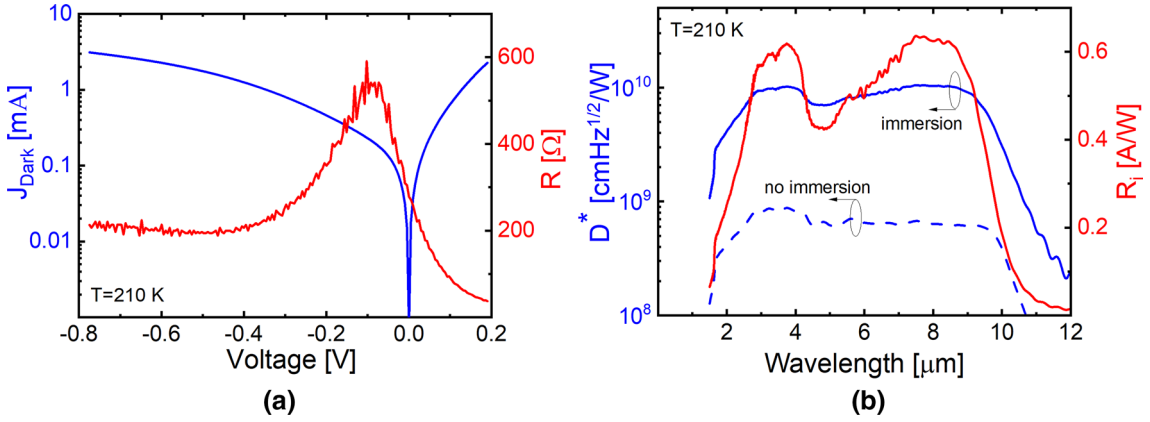

Fig. 3 Dark current and differential resistance (**a**), detectivity and current responsivity (**b**) at 210 K and unbiased condition for LWIR T2SL InAs/InAsSb multi-junction cascade detector with p^+/n^+ connecting regions without immersion lens and supported by GaAs immersion lens.

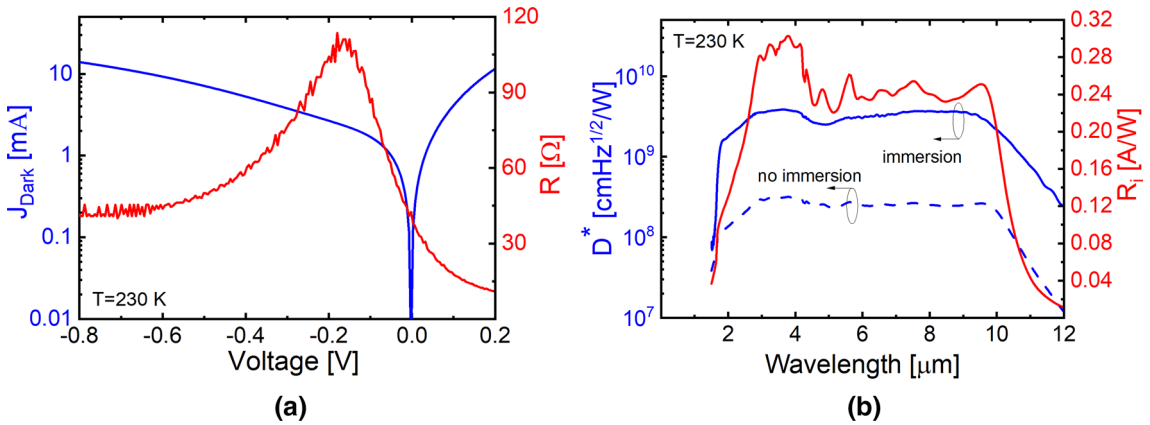

Fig. 4 Dark current and differential resistance (**a**), detectivity and current responsivity (**b**) at 230 K and unbiased condition for LWIR T2SL InAs/InAsSb multi-junction cascade detector with p^+/n^+ connecting regions without immersion lens and supported by GaAs immersion lens.

0.056 A/W while the detectivity reaches 4.2×10^8 cm $Hz^{1/2}/W$ for unbiased conditions, respectively. The detailed comparison of the D^* for selected wavelengths, $\lambda = 2.5$, 4, 6, 8, 10 µm, T and unbiased conditions is presented in the Table I.

An improvement in D^* for the multi-heterojunction device in comparison to the single absorber detector scales versus absorption coefficient and carrier diffusion length product αL according to the relation as:

$$D^*_{\mathrm{ICIP}}/D^*_{\mathrm{Single}} \sim 0.42/(aL)^{1/2}, \quad (2)$$

assuming $\alpha L << 1$.[2] That allows us to estimate the αL product, and subsequently L. For $\lambda_{\mathrm{cut\text{-}off}} \sim 10$ µm, the reported absorption coefficient for LWIR and HOT (210–300 K) ranges from 1400 to 1700 cm^{-1}.[7] To achieve a fully optimized device, the active layer thickness should be 106 nm thick for $T = 300$ K as suggested in Table II, but with a larger number of cascade stages. That number scales versus the absorption coefficient and the single-active-layer thickness product αd could be approximated by the following equations (assuming $\alpha = 166900$ m^{-1} and $d \sim 106$ nm, $T = 300$ K):

- $N_s = (2\alpha d)^{-1}$—when gain is not included—which gives 30;
- $N_s = (1.25\alpha d)^{-1}$—when gain is included—which gives 48.

Figure 6 presents the detectivity performance comparison of the GaAs hyperhemispherically immersed three-stage T2SLs InAs/InAsSb-based detector developed in this work with the T2SLs InAs/GaSb-based ICIPs operating at 300 K, with quantum cascade detectors (QCD) operating at 100 K and multi-junction HgCdTe PVM. In addition, the immersed detector was compared to that without immersion for a wavelength of 10 µm. The medium-wave infrared (MWIR) QCDs reaches $D^* \sim 2\times10^{11}$ cm $Hz^{1/2}/W$ for $\lambda_{\mathrm{Peak}} \sim 4$ µm and $D^* \sim 6\times10^9$ cm $Hz^{1/2}/W$ for $\lambda_{\mathrm{Peak}} \sim 5.75$ µm requiring higher cooling ($T = 100$ K) to operate than ICIPs.[8] Lotfi et al. demonstrated T2SLs InAs/GaSb/$Al_{0.2}In_{0.8}Sb$/GaSb ICIPs reaching $D^* \sim 5.85\times10^9$ cm $Hz^{1/2}/W$ for $\lambda_{\mathrm{Peak}} = 2.1$ µm and

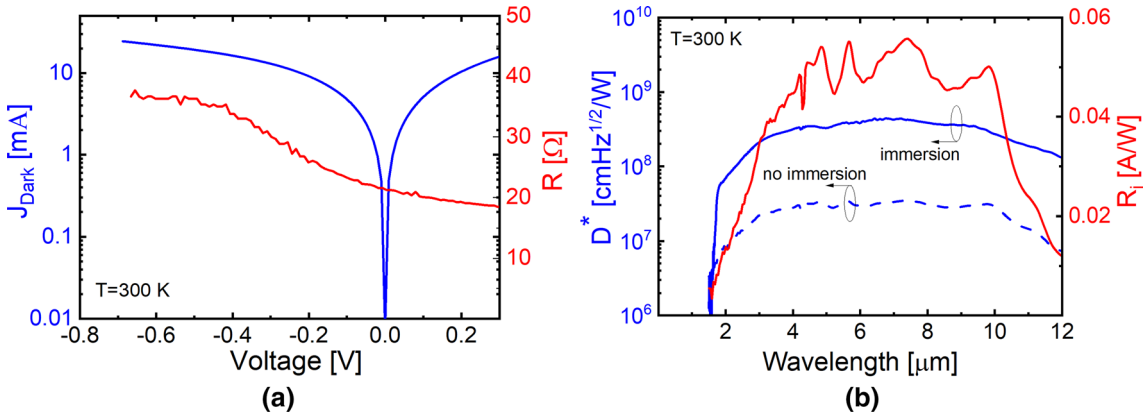

Fig. 5 Dark current and differential resistance (**a**), detectivity and current responsivity (**b**) at 300 K and unbiased condition for LWIR T2SL InAs/InAsSb multi-junction cascade detector with p^+/n^+ connecting regions without immersion lens and supported by GaAs immersion lens.

Table I. The LWIR T2SLs InAs/InAsSb based ICIP detector and single absorber performance for unbiased conditions

T (K)/0 V	N_s	$\lambda_{\mathrm{cut\text{-}off}}$ (µm)	$\lambda_{\mathrm{LWIR\text{-}Peak}}$ (µm)	$\lambda = 2.5$ µm D^* (Jones)	$\lambda = 4$ µm D^* (Jones)	$\lambda = 6$ µm D^* (Jones)	$\lambda = 8$ µm D^* (Jones)	$\lambda = 10$ µm D^* (Jones)
210	1	9.6	7.9	1.01×10^8	1.9×10^8	2.2×10^8	2.9×10^8	1.6×10^8
	3	10.1	7.5	6.1×10^8	8.2×10^8	6.5×10^8	6.4×10^8	3.7×10^8
	3^{im}	10.5	8	6.5×10^9	9.8×10^9	8.4×10^9	1.0×10^{10}	3.1×10^9
230	1	9.8	7.9	3.4×10^7	7.4×10^7	9.2×10^7	1.2×10^8	7.3×10^7
	3	10.3	7.5	1.9×10^8	3.1×10^8	2.5×10^8	2.5×10^8	2.1×10^8
	3^{im}	10.3	7.3	1.3×10^9	3.1×10^9	4.1×10^9	3.5×10^9	1.9×10^9
300	1	10.4	7.9	2.1×10^6	7.6×10^6	1.1×10^7	1.5×10^7	7.3×10^6
	3	10.8	7.5	0.13×10^8	0.28×10^8	0.29×10^8	0.31×10^8	0.292×10^8
	3^{im}	10.8	7.5	1.3×10^8	3×10^8	4×10^8	3.7×10^8	2.8×10^8

3^{im}, GaAs immersed detector; $\lambda_{\mathrm{LWIR\text{-}Peak}}$, peak wavelength within LWIR range

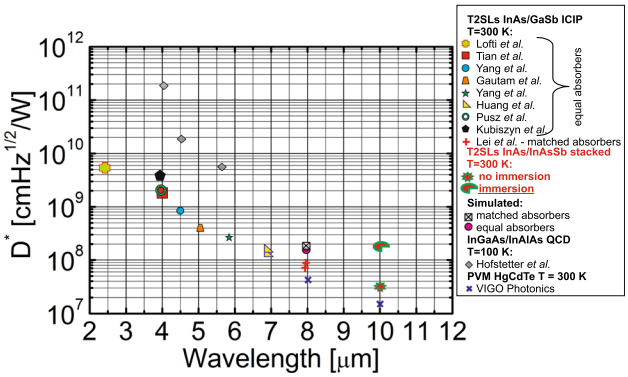

Fig. 6 Detectivity comparison versus wavelength ($\lambda = 2-12$ μm) for T2SLs InAs/InAsSb (without immersion and with GaAs hyperhemispherical immersion lens)-based ICIPs, T2SLs InAs/GaSb equal and matched-absorbers ICIPs, QCD InGaAs/InAlAs and HgCdTe-based multi-junction PVM detectors designed for 300 K.

Table II Calculated carrier diffusion length L for T2SLs InAs/InAsSb absorber layer calculated for $\lambda = 10.6$ μm and $T = 210$, 230, 300 K

T (K)	α (m^{-1})	α L	L (nm)
300	166900	1.78×10^{-2}	106
230	155100	2.22×10^{-2}	143
210	140400	2.89×10^{-2}	206

$T = 300$ K.[9] MWIR equal absorbers ICIPs T2SLs InAs/GaSb were presented by Tian et al., Li et al., Yang et al., Gautam et al. and Kubiszyn et al. (Kubiszyn et al. deposited ICIP on GaAs with a GaSb buffer layer).[10–14] Huang et al. presented a LWIR device with $\lambda_{Peak} = 7$ μm.[15] The LWIR matched-absorber detector was demonstrated by Lei et al. and Hackiewicz et al.[15–17] The matched-absorbers ICIP reaches ~ 10^8 cm $Hz^{1/2}$/W for wavelength $\lambda \sim 8$ μm, twice as high as for the multi-junction PVM HgCdTe operating at 300 K.[18] Comparing the three-stage ICIP T2SLs InAs/InAsSb-based detector with 10.6 μm PVM HgCdTe reaching ~ 1.3×10^7 cm $Hz^{1/2}$/W, the non-immersed ICIP device exhibits ~ 3×10^7 cm $Hz^{1/2}$/W for 300 K. With GaAs immersed, D^* reaches ~ 3×10^8 cm $Hz^{1/2}$/W for 300 K.

Conclusions

The GaAs hyperhemispherically immersed LWIR T2SLs InAs/InAsSb-based cascade photodetector with highly doped p^+/n^+ connecting regions for HOT conditions was designed, grown and processed. Detectivity of the immersed multi-junction heterostructure detector exceeding 10^{10} cm $Hz^{1/2}$/W was measured at wavelength $\lambda \sim 9$ μm and $T = 210$ K [three-stage thermoelectric (TE) cooling] and ~ 3×10^8 cm $Hz^{1/2}$/W $T = 300$ K, achieving a tenfold improvement in detectivity in comparison to the device without an immersion lens and 30-fold improvement in D^* in comparison to the single-stage device with net active layer thickness of 2.2 μm, comparable to the net thickness of the three-stage cascade detector. Comparing the three-stage ICIP T2SLs InAs/InAsSb-based detector with 10.6 μm PVM HgCdTe reaching ~ 1.3×10^7 cm $Hz^{1/2}$/W, the non-immersed ICIP device exhibits ~ 3×10^7 cm $Hz^{1/2}$/W while GaAs-immersed D^* reaches ~ 3×10^8 cm $Hz^{1/2}$/W for 300 K.

Acknowledgements The authors would like to acknowledge the support by the National Science Centre-Poland, Grants: OPUS 2021/34/B/ST7/00768.

Conflict of interest All co-authors have seen and agree with the contents of the manuscript, and there is no conflict of interest to report.

References

1. J. Piotrowski and W. Gawron, Ultimate performance of infrared photodetectors and figure of merit of detector material. *Infrared Phys. Technol.* 38, 63 (1997).
2. R.T. Hinkey and R.Q. Yang, Theory of multiple-stage interband photovoltaic devices and ultimate performance limit comparison of multiple-stage and single-stage interband infrared detectors. *J. Appl. Phys.* 114(10), 104506 (2013).
3. R.Q. Yang and R.T. Hinkey, Ultimate detectivity of multiple-stage interband cascade infrared photodetectors. *Appl. Phys. Lett.* 118, 241101 (2021).
4. R.Q. Yang, Ultimate detectivities of interband cascade infrared photodetectors. in *Proceedings Volume PC12009, Quantum Sensing and Nano Electronics and Photonics XVIII; PC120090G (2022) Event: SPIE OPTO*, 2022, San Francisco, California, United States.
5. P. Martyniuk, A. Rogalski, and S. Krishna, Interband quantum cascade infrared photodetectors: current status and future trends. *Phys. Rev. Appl.* 17, 027001 (2022).
6. W. Gawron, Ł Kubiszyn, K. Michalczewski, J. Piotrowski, and P. Martyniuk, Demonstration of the longwave type-II superlattice InAs/InAsSb cascade photodetector for high operating temperature. *IEEE Electron Device Lett.* 43(9), 1487 (2022).
7. W. Gawron, Ł Kubiszyn, K. Michalczewski, J. Piotrowski, and P. Martyniuk, The performance of the ICIP Ga-free superlattice longwave infrared photodetector for high operating temperature. *Infrared Phys. Technol.* (2022). https://doi.org/10.1016/j.infrared.2022.104499.
8. D. Hofstetter, F.R. Giorgetta, E. Baumann, Q. Yang, C. Manz, and K. Köhler, Mid-infrared quantum cascade detectors for

applications in spectroscopy and pyrometry. *Appl. Phys. B Lasers Opt.* 100(2), 313 (2010).
9. H. Lotfi, L. Li, L. Lei, Y. Jiang, R.Q. Yang, J.F. Klem, and M.B. Johnson, Short-wavelength interband cascade infrared photodetectors operating above room temperature. *J. Appl. Phys.* 119, 2 (2016).
10. R.Q. Yang, Z. Tian, Z. Cai, J.F. Klem, M.B. Johnson, and H.C. Liu, Interband-cascade infrared photodetectors with superlattice absorbers. *J. Appl. Phys.* 107(5), 054514 (2010).
11. N. Gautam, S. Myers, A.V. Barve, B. Klein, E.P. Smith, D.R. Rhiger, L.R. Dawson, and S. Krishna, High operating temperature interband cascade midwave infrared detector based on type-II InAs/GaSb strained layer superlattice. *Appl. Phys. Lett.* 101(2), 3 (2012).
12. Z. Tian, R.T. Hinkey, R.Q. Yang, D. Lubyshev, Y. Qiu, J.M. Fastenau, W.K. Liu, and M.B. Johnson, Iterband cascade infrared photodetectors with enhanced electron barrniers and *p* -type superlattice absorbers. *J. Appl. Phys.* 111(2), 024510 (2012).
13. J.V. Li, R.Q. Yang, C.J. Hill, and S.L. Chuang, Interband cascade detectors with room temperature photovoltaic operation. *Appl. Phys. Lett.* 86(10), 1 (2005).
14. L. Kubiszyn, D. Benyahia, K. Michalczewski, K. Hackiewicz, A. Kębłowski, P. Martyniuk, J. Rutkowski, and J. Piotrowski, Molecular beam epitaxy growth and characterization of interband cascade infrared detectors on GaAs substrates. *J. Cryst. Growth* 534, 125512 (2020).
15. W. Huang, L. Li, L. Lei, J.A. Massengale, R.Q. Yang, T.D. Mishima, and M.B. Santos, Electrical gain in interband cascade infrared photodetectors. *J. Appl. Phys.* 123(11), 113104 (2018).
16. L. Lei, L. Li, H. Ye, H. Lotfi, R.Q. Yang, M.B. Johnson, J.A. Massengale, T.D. Mishima, and M.B. Santos, Long wavelength interband cascade infrared photodetectors operating at high temperatures. *J. Appl. Phys.* 120, 19 (2016).
17. K. Hackiewicz, J. Rutkowski, and P. Martyniuk, Long-wavelength interband cascade detector architectures for room temperature operation. *IEEE J. Quantum Electron.* 55(4), 1 (2019).
18. VIGO PHOTONICS 2020/2021.